nature communications

Article

https://doi.org/10.1038/s41467-025-56488-4

Bimetallic synergy in supported Ni–Pd catalyst for selective hydrogenolysis of C–O bonds in epoxy resins

Received: 30 July 2024

Accepted: 16 January 2025

Published online: 06 February 2025

Check for updates

Yanze Huang[1], Yukari Yamazaki[1], Katsutoshi Nomoto[2], Hiroki Miura[2], Tetsuya Shishido[2], Xiongjie Jin[1] ✉ & Kyoko Nozaki[1] ✉

Recycling of epoxy composites is of importance for achieving circular economy as demand for lightweight materials in the field of sustainable technologies is soaring. Although catalytic hydrogenolysis of epoxy resins provides a promising approach to recover valuable fillers and phenolic compounds from the composites, there is a lack of a reusable solid catalyst for this purpose. Here, we report a robust CeO_2-supported Ni–Pd bimetallic catalyst (Ni–Pd/CeO_2) for the hydrogenolysis of C–O bonds in epoxy resins under 1 atm of H_2. Benefiting from its heterogeneous nature, Ni–Pd/CeO_2 can be reused for several times. Furthermore, the catalyst is successfully applied to decomposition of epoxy composites to recover carbon or glass fibers and phenolic compounds, implying the potential application of our catalyst system toward recycling of epoxy composites.

The growing global concerns about plastic waste contamination have urged our society to develop effective ways to recycle end-of-life plastics[1–4]. Epoxy resins are widely applied in various areas such as construction, electronics, aircraft, automobiles, and wind turbine blades typically in the form of fiber-reinforced epoxy composites (Fig. 1a)[5–7]. Different from thermoplastics such as polyethylene terephthalate, thermosetting epoxy composites are not suitable for mechanical recycling due to the deterioration of material properties, and thus, most of the composites are landfilled, which not only wastes resources but also causes serious environmental problems[8–11]. As the demand for epoxy composites is soaring with the increasing demand for lightweight materials in the field of sustainable technologies such as electric vehicles and wind power plants, the development of efficient approaches to recycle epoxy composites is getting more and more attention for achieving circular economy and carbon neutralization[5–11].

To date, a wide range of methods have been developed for the decomposition of epoxy composites (Fig. 1a)[8–11]. For example, pyrolysis under energy-intensive high-temperature conditions is an approach to recover fillers from the composites, which often causes damage to the fillers due to the harsh conditions[12]. Other methods, such as oxidative decomposition[13–15] using oxidants (e.g., H_2O_2) or solvolysis[16] in concentrated acids (e.g., nitric acid) or bases (e.g., NaOH) have also been developed to deconstruct epoxy resin metrics. However, they have shortcomings of using the undesirable oxidants or a large excess amount of acids or bases which would increase the environmental burden. In addition, all the above methods mainly focus on recovering fillers in the composites, and epoxy resin building blocks such as bisphenol A (BPA) are difficult to recover. In this context, chemical recycling of epoxy resins is of importance to recover valuable fillers together with phenolic compounds from the epoxy composites, but highly challenging due to their inert nature. Recently, it has been revealed that BPA can be recovered from epoxy resins by using a super-stoichiometric amount of potassium or sodium *t*-butoxide (4 equiv. with respect to BPA unit)[17,18] or NaOH (6 equiv. with respect to BPA unit)[19]. However, tedious work-up procedures using a large quantity of acids are necessary to recover BPA because the primary products are potassium or sodium phenolates.

Quite recently, catalytic reductive decomposition has emerged as a promising method to recover fillers and phenolics from epoxy

[1]Department of Chemistry and Biotechnology, Graduate School of Engineering, The University of Tokyo, Tokyo, Japan. [2]Department of Applied Chemistry for Environment, Graduate School of Urban Environmental Sciences, Tokyo Metropolitan University, Tokyo, Japan. ✉e-mail: t-jin@g.ecc.u-tokyo.ac.jp; nozaki@chembio.t.u-tokyo.ac.jp

https://doi.org/10.1038/s41467-025-56488-4

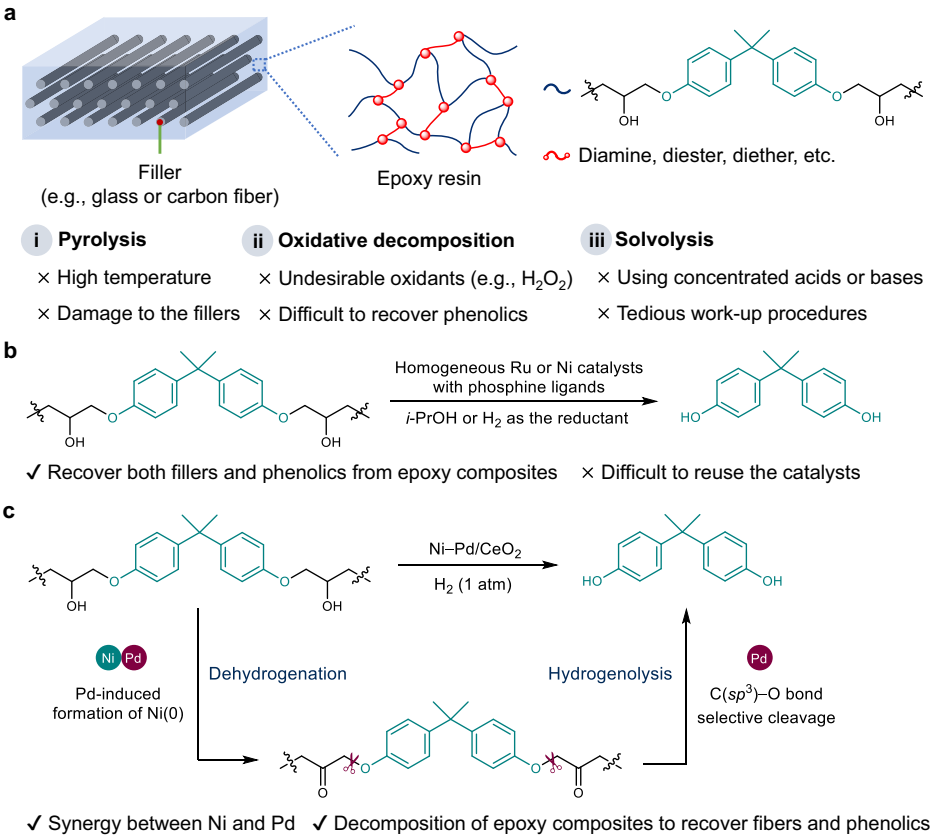

Fig. 1 | Outline of this work. a Structure of typical epoxy resin composites and traditional methods for their decomposition. **b** Previous works: hydrogenolysis of epoxy resins using homogeneous Ru or Ni catalysts with phosphine ligands. **c** This work: hydrogenolysis of epoxy resins by a reusable Ni–Pd/CeO_2 catalyst enabled by the synergy between Ni and Pd.

composites (Fig. 1b)[20–22]. For example, Ahrens and Skrydstrup have reported a homogeneous Ru/triphos (triphos = 1,1,1-tris(diphenylphosphinomethyl)ethane) catalyst for decomposition of epoxy resin composites to recover fibers and BPA using 2-propanol as the hydrogen source[20,21]. Concurrently, our group has developed a homogeneous Ni/dcype (dcype = 1,2-bis(dicyclohexylphosphino)ethane) catalyst for hydrogenolysis of epoxy resins to recover BPA using H_2 as the reductant[22]. In spite of the efficiency of these catalyst systems for recovering BPA and fibers from epoxy composites, they suffer from difficulties in catalyst recovery and reuse due to their homogeneous nature. Thus, homogeneous catalysts are not practical for the decomposition of large-scale epoxy composites especially when noble metal catalysts and/or expensive ligands are employed. Therefore, the development of a robust and reusable heterogeneous catalyst for hydrogenolysis of epoxy resins to recycle epoxy composites is highly desirable from a practical point of view. However, as far as we know[8–22], there is a lack of a heterogeneous catalyst for decomposition of epoxy composites to recover phenolics and fillers.

Considering most epoxy resins utilized nowadays are prepared by curing the BPA-based epoxide prepolymer with amines or acid anhydrides (Fig. 1a)[5–7,23,24], the key to recover BPA is the selective hydrogenolysis of C(sp^3)–O bonds in the alkyl phenyl ether moiety without over reduction of aromatic rings[25–36]. To achieve this purpose, we considered exploring bimetallic catalysts with the expectation that synergy between two metals could substantially enhance the catalytic performance for the selective hydrogenolysis of C(sp^3)–O bonds in epoxy resin backbone compared to the corresponding single metallic catalysts[37–48]. Here, for the first time, we successfully developed a reusable CeO_2-supported Ni–Pd bimetallic catalyst (Ni–Pd/CeO_2) for the hydrogenolysis of epoxy resins under 1 atm of H_2 (Fig. 1c). Mechanistic studies suggested that Pd induces the formation of Ni(0) species to facilitate dehydrogenation of alcohol moieties in epoxy resin backbone and that the selective cleavage of C(sp^3)–O over C(sp^2)–O bond is mainly promoted by Pd species. By using the present catalyst system, we demonstrate the mild decomposition of epoxy composites, including carbon fiber-reinforced plastics (CFRPs) and circuit boards, to recover carbon or glass fibers and phenolic compounds, implying its potential application to recycle epoxy composites.

Results and discussion

Catalyst development

Initially, the Ni–Pd/CeO_2 catalyst with the Ni to Pd ratio of 1/1 (Ni_1Pd_1/CeO_2) was prepared by deposition-precipitation method followed by treatment with 1 atm of H_2 at 150 °C for 0.5 h (the supported metal catalysts are designated as $M_xM'_y$/support, where the ratio of M to M′ is x/y; see Supplementary Information for the details on the catalyst preparation). Then, Ni_1Pd_1/CeO_2 was applied to the hydrogenolysis of epoxy resin model **1** in *N*-methylpyrrolidone (NMP) at 180 °C and under 1 atm of H_2. In this case, BPA (**2**), 4-isopropylphenol (**3**) and phenol (**4**) were obtained in 76%, 16% and 14% yields, respectively (Table 1, entry 1). When the reaction time was extended to 48 h, further cleavage of C–C bond proceeded and the yields of **3** and **4** increased to 81% and 59%, respectively (Table 1, entry 2). Other bimetallic catalysts such as Cu_1Pd_1/CeO_2, Co_1Pd_1/CeO_2, Fe_1Pd_1/CeO_2, Mn_1Pd_1/CeO_2, Ni_1Pt_1/CeO_2, and Fe_1Pt_1/CeO_2 showed much lower activity than Ni_1Pd_1/CeO_2 (Table 1, entries 3–8). Interestingly, the aromatic rings of phenolic products were not hydrogenated. The conversion of **1** and the yields of phenolic products gradually increased with increasing the amount of the supported Pd species

https://doi.org/10.1038/s41467-025-56488-4

Table 1 | Effect of catalysts on the hydrogenolysis of epoxy resin model 1

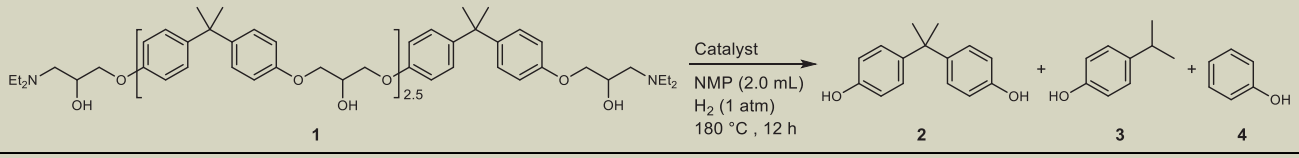

Entry[a]	Catalyst	Conv. of 1 (%)	Yield (%)		
			2	3	4
1[b]	Ni_1Pd_1/CeO_2	95	76	16	14
2[c]	Ni_1Pd_1/CeO_2	99	16	81	59
3	Cu_1Pd_1/CeO_2	25	19	1	n.d.
4	Co_1Pd_1/CeO_2	41	25	12	11
5	Fe_1Pd_1/CeO_2	45	21	n.d.	n.d.
6	Mn_1Pd_1/CeO_2	49	38	3	3
7	Ni_1Pt_1/CeO_2	17	14	n.d.	n.d.
8	Fe_1Pt_1/CeO_2	22	6	n.d.	n.d.
9	$Ni_1Pd_{0.1}/CeO_2$	28	12	n.d.	n.d.
10	$Ni_1Pd_{0.5}/CeO_2$	51	36	2	n.d.
11	Ni_1Pd_4/CeO_2	15	10	3	2
12[b]	$Ni_{0.5}Pd_1/CeO_2$	95	73	14	12
13[b]	Ni_2Pd_1/CeO_2	96	76	13	8
14[b]	Ni_4Pd_1/CeO_2	97	66	16	12
15[d]	Ni/CeO_2	11	1	n.d.	n.d.
16[e]	Pd/CeO_2	18	9	2	1
17	Ni_1Pd_1/TiO_2	25	6	n.d.	n.d.
18	Ni_1Pd_1/Al_2O_3	11	4	n.d.	n.d.
19	Ni_1Pd_1/ZrO_2	5	1	n.d.	n.d.
20[d,e]	$Ni/CeO_2 + Pd/CeO_2$	49	29	4	4
21[f]	CeO_2	3	n.d.	n.d.	n.d.

[a]Reaction conditions: **1** (200 mg, 0.52 mmol BPA unit), $M_xM'_y/CeO_2$ (100 mg; M ≈ 4.2*x* mol%; M′ ≈ 4.8*y* mol%, the exact amount of the metal used in the hydrogenolysis is varied slightly depending on the kind of supported metal species), NMP (2.0 mL), 180 °C, H_2 (1 atm, balloon), 12 h. All the supported metal catalysts were pre-treated with 1 atm of H_2 at 150 °C for 0.5 h. Conversion of **1** and yield of **4** were determined by ^{1}H NMR analysis. Yields of **2** and **3** were determined by GC analysis. [b]An average value of two parallel experiments is shown here, and standard deviations are <4% for all data points, see Supplementary Table 1 for details. n.d. = not detected.
[c]48 h.
[d]Ni/CeO_2 (100 mg, Ni = 4.0 mol%).
[e]Pd/CeO_2 (100 mg, Pd = 5.0 mol%).
[f]CeO_2 (100 mg).

(Table 1, entries 1, 9, and 10). However, a further increase resulted in a decrease in the catalytic activity (Table 1, entry 11). In contrast, there is no substantial change in the conversion or yields when the amount of Ni increased or decreased (Table 1, entries 1, 12–14). The single metallic Ni/CeO_2 or Pd/CeO_2 was much less effective than the Ni–Pd bimetallic catalysts for the hydrogenolysis and gave significantly lower yields of the corresponding phenolic products (Table 1, entries 15 and 16). Ni–Pd supported on other supports, such as TiO_2, Al_2O_3, or ZrO_2, resulted in much lower conversion and yields than Ni_1Pd_1/CeO_2 (Table 1, entries 17–19). Furthermore, a physical mixture of Ni/CeO_2 and Pd/CeO_2 resulted in higher activity than Ni/CeO_2 or Pd/CeO_2 alone (Table 1, entry 20 vs 15 or 16), but still gave much lower conversion and yields than Ni_1Pd_1/CeO_2 (Table 1, entry 20 vs 1). Therefore, only if Ni together with Pd were directly supported on CeO_2, the activity for the hydrogenolysis increased dramatically, and the synergy between Ni and Pd is crucial for the high activity of Ni_1Pd_1/CeO_2. As a control experiment, CeO_2 did not promote the hydrogenolysis of **1** (Table 1, entry 21). Solvent effects on the hydrogenolysis of **1** were also investigated. Among various solvents examined such as NMP, cyrene, γ-valerolactone, 1,3-dimethyl-2-imidazolidinone, and triglyme, NMP resulted in the highest conversion and yields (Supplementary Table 2).

Characterization of the catalyst

The Ni_1Pd_1/CeO_2 catalyst was characterized by powder X-ray diffraction (XRD), X-ray photoelectron spectroscopy (XPS), X-ray absorption fine structure (XAFS) spectroscopy, and high-angle annular dark-field scanning transmission electron microscopy (HAADF-STEM) analysis. XRD pattern of the catalyst revealed that the structure of CeO_2 was maintained well upon immobilization of Ni and Pd species and the subsequent treatment with H_2 gas (Fig. 2a). Furthermore, no apparent diffraction peaks attributable to Pd, Ni, or NiO were observed, indicating Ni and Pd species are highly dispersed on CeO_2 surface (Fig. 2a). From the X-ray photoelectron spectroscopy (XPS) analysis of Ni_1Pd_1/CeO_2, the supported Ni–Pd alloy nanoparticles contain Pd^{2+} (336.8 and 342.2 eV), Pd^0 (335.2 and 340.5 eV), Ni^{2+} (855.4 eV), and Ni^0 (852.4 eV) species, and the ratios of Pd^{2+} to Pd^0 and Ni^{2+} to Ni^0 were 17/83 and 79/21, respectively (Fig. 2b, c). Pd K-edge X-ray absorption near edge structure (XANES) spectrum of Ni_1Pd_1/CeO_2 showed that the supported Pd is mainly composed of Pd^0 species (Fig. 2d). From Ni K-edge XANES spectrum, it is revealed that the catalyst mainly contains Ni^{2+} species (Fig. 2e). Therefore, the results obtained from XANES spectra are in good agreement with those from XPS spectra. HAADF-STEM and EDS analysis of the catalyst showed that Ni and Pd species are located on the same position of the catalyst

https://doi.org/10.1038/s41467-025-56488-4

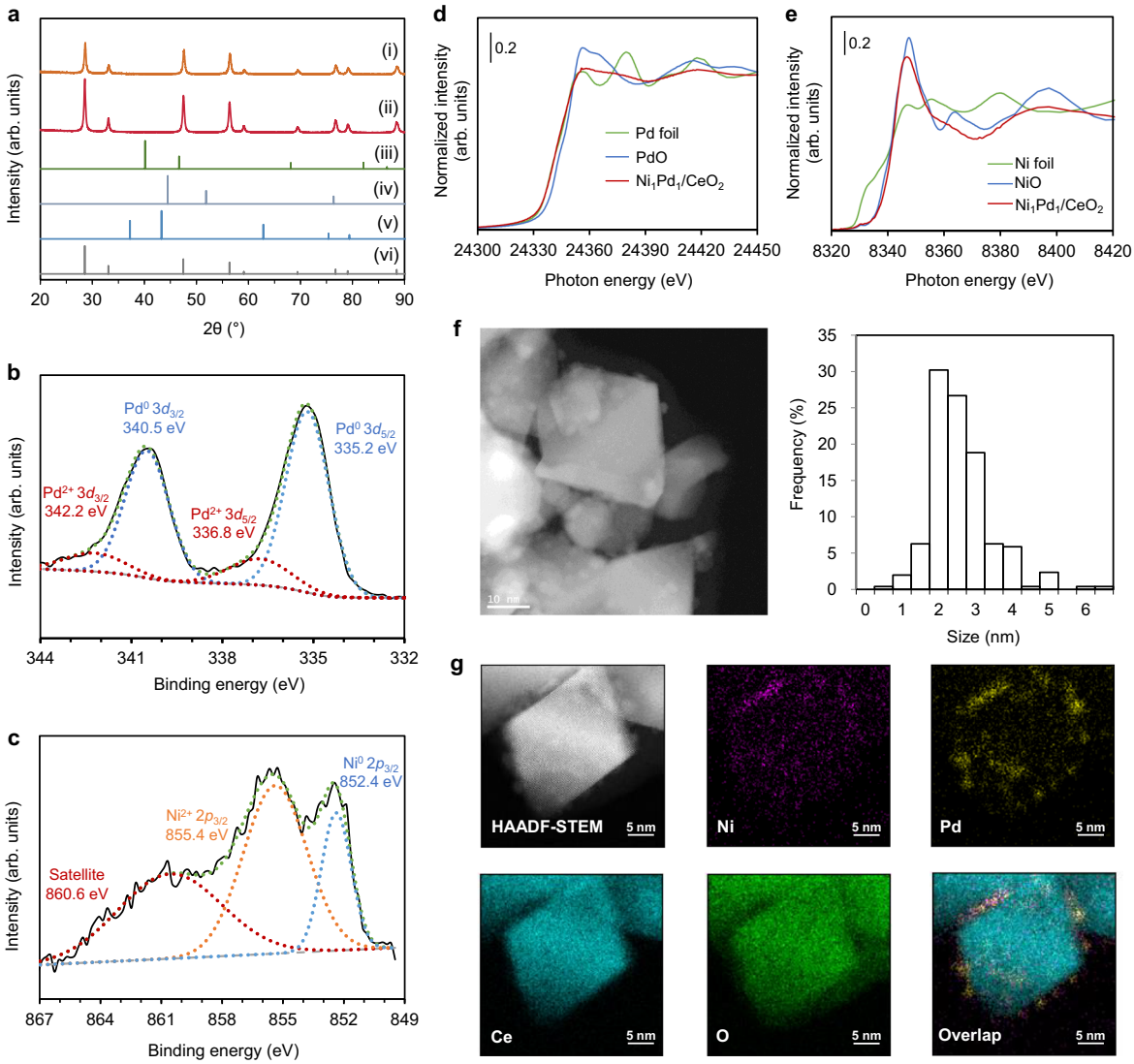

Fig. 2 | Characterization of Ni_1Pd_1/CeO_2. **a** XRD patterns of (i) Ni_1Pd_1/CeO_2, (ii) CeO_2, (iii) the powder diffraction file of Pd metal (file No. 8796), (iv) the powder diffraction file of Ni metal (file No. 8783), (v) the powder diffraction file of NiO (file No. 5898), and (vi) the powder diffraction file of CeO_2 (file No. 11). **b** XPS spectrum of Ni_1Pd_1/CeO_2 in the region of 332–344 eV (Pd 3*d*). **c** XPS spectrum of Ni_1Pd_1/CeO_2 in the region of 849–867 eV (Ni 2*p*). The black line indicates the original spectrum, the blue, red, and orange broken lines indicate the deconvoluted signals and the green broken line indicates the sum of the deconvoluted signals. **d** Pd K-edge XANES spectrum. **e** Ni K-edge XANES spectrum. **f** STEM image and particle size distribution of Ni_1Pd_1/CeO_2 (average = 2.6 nm; standard deviation, σ = 0.8 nm, n = 256). **g** HAADF-STEM image and elemental mapping of Ni_1Pd_1/CeO_2 by EDS analysis. For the above analyses, Ni_1Pd_1/CeO_2 was pre-treated with 1 atm of H_2 at 150 °C for 0.5 h.

surface, and the average particle size was approximately 2.6 nm (Fig. 2f, g).

Hydrogenolysis of other epoxy resin model compounds by Ni_1Pd_1/CeO_2

As shown in Fig. 3, Ni_1Pd_1/CeO_2 can efficiently promote the hydrogenolysis of various epoxy model compounds. For model compounds **5**–**7** having hydroxy group adjacent to the ether bonds, the hydrogenolysis proceeded smoothly under 1 atm of H_2, giving the corresponding hydrogenolysis product **9** in high yields (Fig. 3). When the hydrogenolysis of **5** was carried out in the presence of tributylamine, substantial amounts of the C–C bond-cleaved products such as **3** (45%), **4** (13%), and anisole (29%) were obtained (Supplementary Fig. 1). Therefore, the amine moiety in model **1** is likely the reason for the formation of **3** and **4** for the hydrogenolysis of **1** (Table 1, entry 1).

The hydrogenolysis of models **5**–**7** also proceeded under N_2 with lower yields of **9** produced, indicating the transfer hydrogenolysis proceeded for which the hydroxy groups would serve as the hydrogen source. In addition, the hydrogenolysis of the ether without the hydroxy group did not proceed at all, suggesting that the hydroxy group is necessary for the efficient hydrogenolysis of the ether bonds (Fig. 3, model **8**). Nevertheless, we found that the hydrogenolysis of model **8** proceeded to some extent by adding a base such as K_3PO_4, though the conversion was much lower than other models having the hydroxy group (Supplementary Fig. 2). The effect of the hydroxy group on the hydrogenolysis is discussed in the following section.

Mechanistic studies

The reaction pathway for the present hydrogenolysis was investigated. As mentioned above, the hydrogenolysis of models **5**–**7** proceeded even under N_2 and model **8** did not react at all (Fig. 3). Therefore, it is likely that the hydrogenolysis proceeds through dehydrogenation of the alcohol moiety to form the corresponding ketone intermediate (Fig. 4a, step 1) followed by hydrogenolysis of the C–O bond adjacent

https://doi.org/10.1038/s41467-025-56488-4

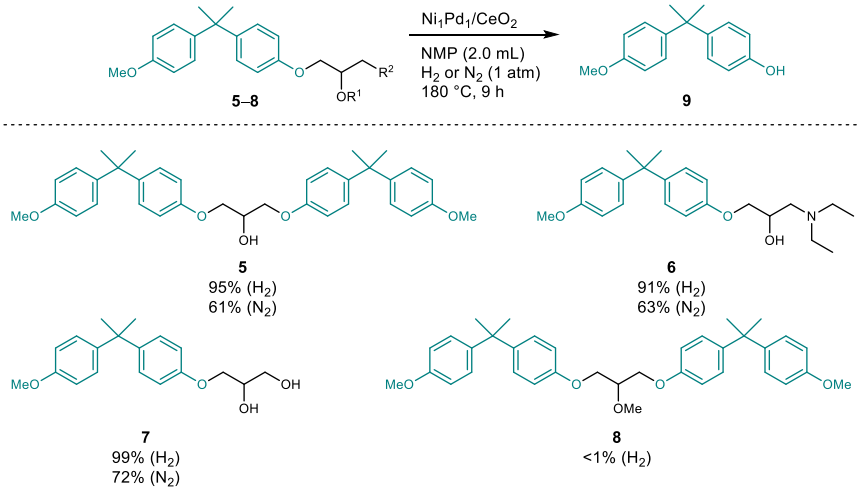

Fig. 3 | Hydrogenolysis of various epoxy resin model compounds by Ni_1Pd_1/CeO_2. Reaction conditions: model **5** or **8** (0.25 mmol), Ni_1Pd_1/CeO_2 (100 mg), NMP (2.0 mL), 180 °C, H_2 (1 atm, balloon), 9 h. For model **6** or **7**, 0.50 mmol of the substrate was used. The catalyst was pre-treated with 1 atm of H_2 at 150 °C for 0.5 h. The yields of **9** are shown here for the hydrogenolysis of each model compound under H_2 or N_2. The yields were determined by GC analysis.

to the carbonyl group (Fig. 4a, step 2). The proposed reaction pathway was further supported by the hydrogenolysis of models **10** and **11** (Fig. 4b). When the hydrogenolysis of **10** was carried out at 180 °C and under 1 atm of H_2 for 6 h, full conversion of **10** gave **9**, 2-tetradecanone (**12**), and 2-tetradecanol (**13**) in 91%, 80%, and 14% yield, respectively (Fig. 4b (i), entry 1). Notably, when Ni/CeO_2 was used as the catalyst, the dehydrogenated ketone intermediate **11** was detected (Fig. 4b (i), entry 3). In addition, the hydrogenolysis of **11** using Ni_1Pd_1/CeO_2 proceeded smoothly (Fig. 4b (ii), entry 1). Therefore, the reaction proceeds through the ketone intermediate as shown in Fig. 4a. Also, the formation of **10** during the hydrogenolysis of **11** suggests that an equilibrium between **10** and **11** exists via dehydrogenation and hydrogenation (Fig. 4b (ii), entries 1 and 3).

Next, the role of the supported Ni and Pd species for the hydrogenolysis was investigated. For the hydrogenolysis of **11** using catalysts pre-treated with 1 atm H_2 at 300 °C, Pd/CeO_2 resulted in almost the same conversion and yields as Ni_1Pd_1/CeO_2 (Fig. 4b (ii), entry 1 vs entry 2), but is much more active than Ni/CeO_2 (Fig. 4b (ii), entry 2 vs entry 3). Even for Ni/CeO_2 pre-treated at 400 °C, which has almost the same ratio of Ni^0 species (53%, Supplementary Fig. 3) as Ni_1Pd_1/CeO_2 pre-treated at 300 °C (51%, Fig. 4c (iii)), the activity was still much lower than Pd/CeO_2 (Fig. 4b (ii), entry 2 vs entry 4). These results indicate that the supported Pd species are highly active and mainly responsible for the hydrogenolysis of the ketone intermediate (Fig. 4a, step 2). On the other hand, Pd/CeO_2 showed much lower activity than Ni_1Pd_1/CeO_2 for the hydrogenolysis of **10** (Fig. 4b (i), entry 1 vs entry 2), which suggests the Pd species alone have lower efficiency for the dehydrogenation step, and Ni together with Pd substantially promote the dehydrogenation of **10** to **11** (Fig. 4a, step 1).

For the hydrogenolysis of model **5**, an induction period was observed (Fig. 4c (i), and Supplementary Fig. 4). To investigate the origin of the induction period, we pre-treated Ni_1Pd_1/CeO_2 with 1 atm of H_2 at different temperatures, and the hydrogenolysis of **5** was carried out using these catalysts. The reaction profiles showed that the induction period was decreased with an increase in the pre-treatment temperature (Fig. 4c (i)). XPS analysis of the catalysts showed that the ratio of Pd^{2+} to Pd^0 was approximately the same when the catalyst was treated at different temperatures (Fig. 4c (ii)). However, the ratio of Ni^{2+} to Ni^0 decreased from 79/21 to 49/51, indicating a substantially larger amount of Ni^{2+} species was reduced to Ni^0 at higher pre-treatment temperature (Fig. 4c (iii)). Therefore, the supported Ni species rather than Pd species are related to the induction period, and the higher amount of the surface Ni^0 species resulted in a shorter induction period. This result was further supported by the following experiments. When Ni_1Pd_1/CeO_2 pre-treated with H_2 at 150 °C was subjected to the hydrogenolysis of **5** and recovered after 2 h, the ratio of Ni^{2+} to Ni^0 was decreased from 79/21 to 57/43, and the ratio was kept almost unchanged until the end of the reaction (61/39), supporting that Ni^{2+} was reduced to Ni^0 during the induction period (Supplementary Fig. 5).

In our bimetallic catalyst system, Pd induces the reduction of Ni^{2+} to Ni^0. When Ni/CeO_2 was reduced with 1 atm of H_2 at 300 °C for 1 h, the ratio of Ni^{2+} to Ni^0 was 73/27 (Supplementary Fig. 6). On the other hand, the ratio was 49/51 for Ni_1Pd_1/CeO_2 reduced under the same conditions, indicating a larger amount of Ni^{2+} was reduced to Ni^0 in the presence of Pd. As the supported Pd species rather than Ni species play the major role in the hydrogenolysis of the C–O bond in the ketone intermediate **11**, the reduction of Ni^{2+} to Ni^0 is indispensable for promoting the dehydrogenation of the alcohol moiety. Overall, the Pd-induced reduction of Ni^{2+} to Ni^0 enhances the rate of the dehydrogenation step shown in Fig. 4a. Consequently, the bimetallic Ni_1Pd_1/CeO_2 is much more active than the corresponding single metallic catalysts for the hydrogenolysis of the β-hydroxy ether moieties in epoxy resins.

Hydrogenolysis of epoxy resins

The applicability of our catalyst system was demonstrated by the hydrogenolysis of epoxy resins and the decomposition of epoxy composites. As shown in Fig. 5, Ni_1Pd_1/CeO_2 was successfully applied to the hydrogenolysis of acid anhydride- or amine-cured epoxy resins. For the hydrogenolysis of the BPA-based epoxy resin cured with 4-methylhexahydrophthalic anhydride (MHHPA), a catalytic amount of 1,8-diazabicyclo[5.4.0]undec-7-ene (DBU) was added to promote decomposition[49], and BPA was obtained in 52% yield (Fig. 5a). The hydrogenolysis of the BPA-based epoxy resin cured with 4,4′-methylenebis(cyclohexylamine) (MBCHA) also proceeded efficiently in the presence of a catalytic amount of K_3PO_4 (Fig. 5b). In this case, C–C bond cleavage occurred to give 4-isopropylphenol and phenol in 99% and 81% yield, respectively. As described above, the aliphatic tertiary amine moiety in the epoxy resin is likely responsible for the C–C bond cleavage. Considering the hydroxy groups in the resin are often involved in crosslinking, the role of K_3PO_4 in our catalyst system is likely to promote the hydrogenolysis of the ether bond even without the β-hydroxy group, which is supported by the experimental result

https://doi.org/10.1038/s41467-025-56488-4

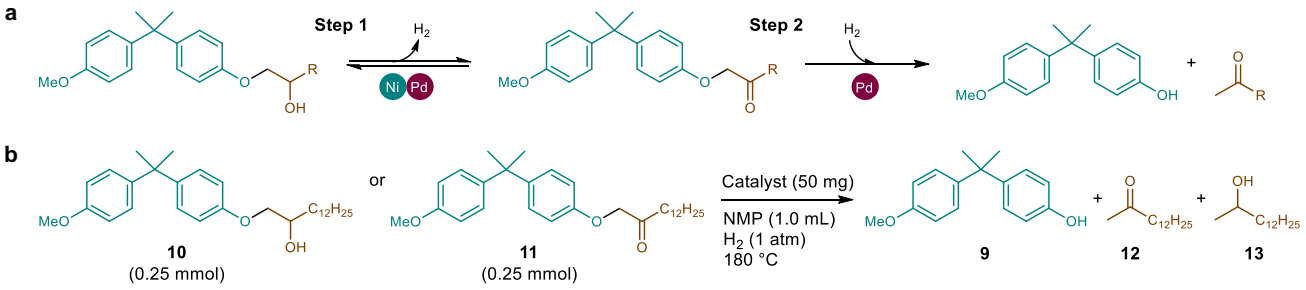

i **Model 10 as the substrate (reaction time = 6 h)**

Entry	Catalyst	Conv. of **10** (%)	Yield (%)			
			9	**12**	**13**	**11**
1[a]	Ni_1Pd_1/CeO_2	>99	91	80	14	n.d.
2[a]	Pd/CeO_2	24	23	21	1	n.d.
3[a]	Ni/CeO_2	17	5	2	n.d.	12
4[b]	Ni/CeO_2	16	4	2	n.d.	11

ii **Model 11 as the substrate (reaction time = 4 h)**

Entry	Catalyst	Conv. of **11** (%)	Yield (%)			
			9	**12**	**13**	**10**
1[a]	Ni_1Pd_1/CeO_2	>99	94	86	8	5
2[a]	Pd/CeO_2	94	85	87	n.d.	n.d.
3[a]	Ni/CeO_2	76	8	7	1	68
4[b]	Ni/CeO_2	68	13	11	n.d.	42

[a]The catalyst was treated with 1 atm of H_2 at 300 °C for 1 h. [b]The catalyst was treated with 1 atm of H_2 at 400 °C for 3 h. Conversion or yield of **10** and **11** was determined by ^{1}H NMR analysis. Yields of **9**, **12**, and **13** were determined by GC analysis. n.d. = not detected.

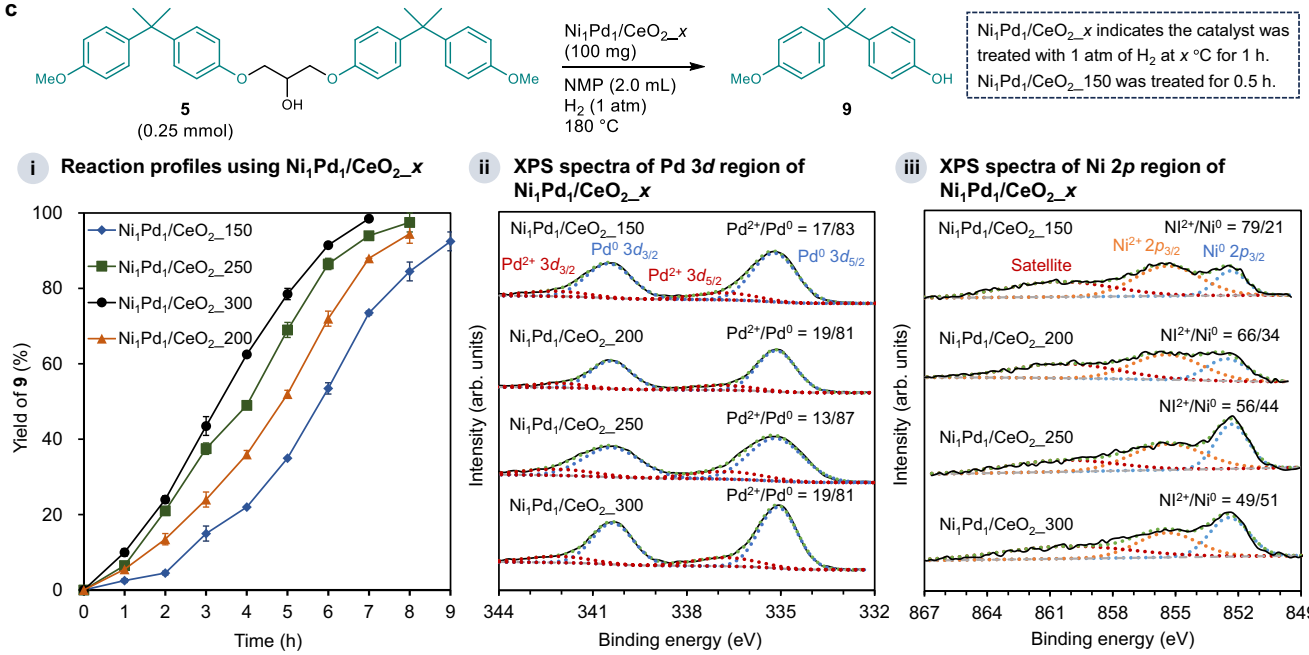

Fig. 4 | Mechanistic studies. a Proposed reaction pathway for the hydrogenolysis. **b** Hydrogenolysis of models **10** and **11** using Ni_1Pd_1/CeO_2, Pd/CeO_2, or Ni/CeO_2. **c** The hydrogenolysis of model **5** using Ni_1Pd_1/CeO_2 pre-treated at different temperatures. (i) reaction profiles (each data point represents an average value of two parallel experiments, and standard deviations were added as error bars), (ii) XPS spectra of the catalysts in Pd 3*d* region, and (iii) XPS spectra of the catalysts in Ni 2*p* region. The black line indicates the original spectrum, the blue, red, and orange broken lines indicate the deconvoluted signals and the green broken line indicates the sum of the deconvoluted signals.

that hydrogenolysis of model **8** indeed proceeded in the presence of K_3PO_4 (Supplementary Fig. 2). The hydrogenolysis of commercial BPA-based epoxy resins cured with amines other than MBCHA (Supplementary Table 3) and bisguaiacol F (BGF)-based epoxy resin cured with MBCHA (Supplementary Fig. 7) also proceeded to give the corresponding phenolic products. Scale-up of the hydrogenolysis was also successful. As shown in Fig. 5a, b, the corresponding phenolic products were formed in yields comparable to the small-scale hydrogenolysis, and the products were successfully isolated using silica gel column chromatography. Moreover, the present catalyst system was also applicable to the bisphenol S (BPS)-based epoxy resin, giving BPS in 39% isolated yield (Fig. 5c). Control experiments using base additives in the absence of Ni_1Pd_1/CeO_2 resulted in the formation of much lower yields of phenolic products (<15% yields, Supplementary Table 4), indicating Ni_1Pd_1/CeO_2 is indispensable for the hydrogenolysis.

Decomposition of epoxy composites

The present catalyst system can be applied to the decomposition of epoxy composites. For example, CFRPs composed of carbon fibers and epoxy resins cured with methylcyclohexene-1,2-dicarboxylic anhydride (CFRP_MCDA) or dicyandiamide (CFRP_DICY) were successfully decomposed, and carbon fibers and phenolics were recovered from the CFRPs (Fig. 6a, b). The recovered carbon fibers were analyzed by scanning electron microscope (SEM), which revealed that the carbon

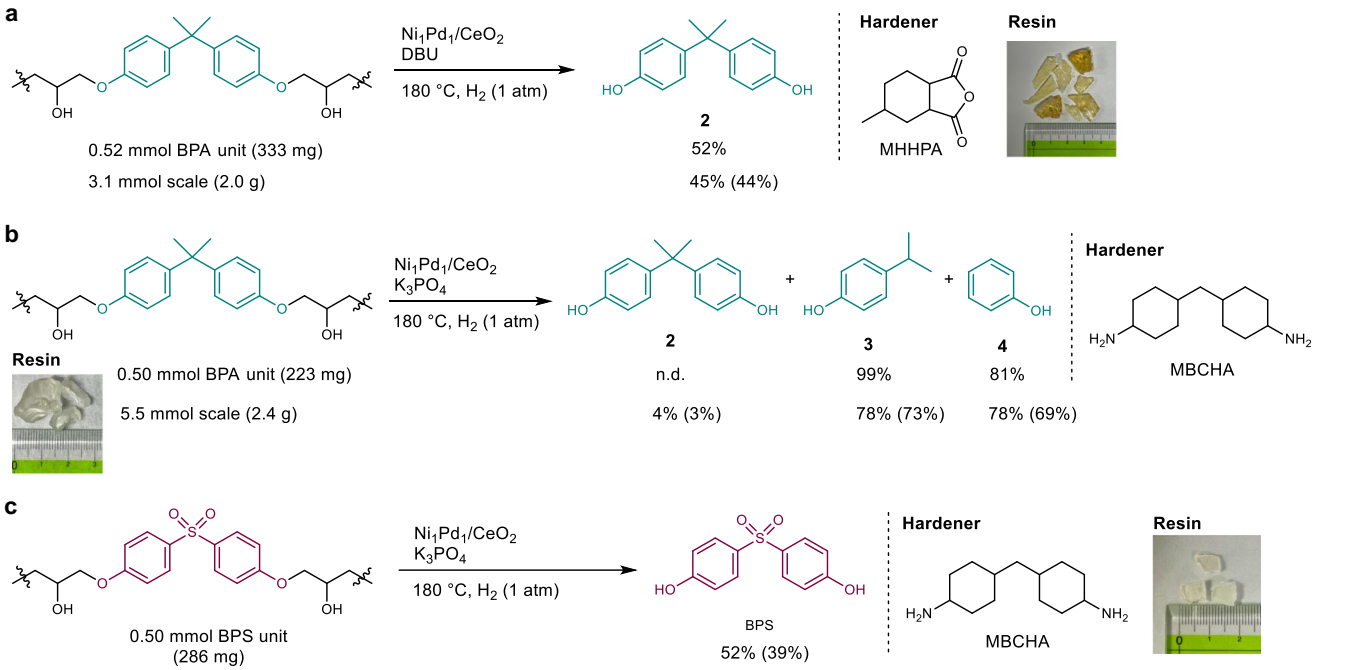

Fig. 5 | Ni_1Pd_1/CeO_2-catalyzed hydrogenolysis of epoxy resins. a Hydrogenolysis of the BPA-based epoxy resin cured with MHHPA. Reaction conditions (0.52 mmol scale): resin (chunks, 333 mg, 0.52 mmol BPA unit), Ni_1Pd_1/CeO_2 (100 mg), DBU (0.125 mmol), NMP (1.0 mL), 180 °C, H_2 (1 atm, balloon), 7 d. Reaction conditions (3.1 mmol scale): resin (chunks, 2.0 g, 3.1 mmol BPA unit), Ni_1Pd_1/CeO_2 (500 mg), DBU (1.0 mmol), NMP (5.0 mL), 180 °C, H_2 (1 atm, balloon), 7 d. **b** Hydrogenolysis of the BPA-based epoxy resin cured with MBCHA. Reaction conditions (0.50 mmol scale): resin (powder, 223 mg, 0.50 mmol BPA unit), Ni_1Pd_1/CeO_2 (100 mg), K_3PO_4 (0.125 mmol), NMP (1.0 mL), 180 °C, H_2 (1 atm, balloon), 3 d. Reaction conditions (5.5 mmol scale): resin (chunks, 2.4 g, 5.5 mmol BPA unit), Ni_1Pd_1/CeO_2 (500 mg), K_3PO_4 (0.60 mmol), NMP (5.0 mL), 180 °C, H_2 (1 atm, balloon), 3 d. **c** Hydrogenolysis of the BPS-based epoxy resin cured with MBCHA. Reaction conditions: resin (chunks, 286 mg, 0.50 mmol BPS unit), Ni_1Pd_1/CeO_2 (100 mg), K_3PO_4 (0.125 mmol), NMP (1.0 mL), 180 °C, H_2 (1 atm, balloon), 3 d. For all the above experiments, Ni_1Pd_1/CeO_2 was pre-treated with 1 atm of H_2 at 300 °C for 1.0 h. Yields of BPA, 4-isopropylphenol, and phenol were determined by GC analysis, and BPS by ^{1}H NMR. Isolated yields are shown in parentheses. Pictures of epoxy resin substrates are also shown. Synthetic procedures for the epoxy resins are shown in the Supplementary methods.

fiber surface was clean after the decomposition (Fig. 6a, b). Furthermore, decomposition of a circuit board composed of epoxy resins and glass fibers was also successful, and glass fibers and phenolic products **3** and **4** were recovered (Fig. 6c). From SEM analysis of the recovered fibers, it was revealed that the fiber surface was quite clean (Fig. 6c). For the decomposition of CRFPs or the circuit board, although decomposition proceeded using base in the absence of the catalyst, the yields of recovered phenolics were much lower (Supplementary Fig. 8). In addition, although the surface of fibers recovered from CFRP_MCDA was clean, those from CFRP_DICY and the circuit board were not. Therefore, Ni_1Pd_1/CeO_2 is necessary for recovering phenolics and/or clean fibers.

Verification of heterogeneous nature and reuse experiment of Ni_1Pd_1/CeO_2

The heterogeneous nature of the present catalyst system was investigated as follows. For the hydrogenolysis of **5** under the conditions shown in Fig. 7, the reaction completely stopped when the catalyst was removed by hot filtration at the conversion of approximately 60% (Fig. 7a). In addition, when the filtrate obtained after the hydrogenolysis was analyzed by inductively coupled plasma optical emission spectroscopy (ICP-OES), Ni and Pd species were hardly detected (below the detection limit). Therefore, the Ni_1Pd_1/CeO_2 catalyst worked as a heterogeneous catalyst and the reaction proceeded on the catalyst surface[50].

Then, the reusability of Ni_1Pd_1/CeO_2 was examined for the hydrogenolysis of **5**. The catalyst can be easily retrieved from the reaction mixture by simple filtration with >95% recovery after the hydrogenolysis. The recovered catalyst was washed with acetone, water, and ethanol followed by drying at room temperature and reducing with 1 atm of H_2 at 300 °C for 1 h before each reuse experiment. As shown in Fig. 7b, the catalyst can be reused at least five times without significant loss of performance. The HAADF-STEM analysis of Ni_1Pd_1/CeO_2 recovered after the 5th reuse experiment revealed that the Ni–Pd alloy nanoparticles remain highly dispersed on the CeO_2 surface without significant aggregation of particles (Supplementary Fig. 9). Furthermore, by comparing the powder XRD patterns of the fresh Ni_1Pd_1/CeO_2 and that recovered after the 5th reuse experiment, the structure of the CeO_2 support remained unchanged (Supplementary Fig. 10). These results support the robustness of Ni_1Pd_1/CeO_2 for the hydrogenolysis.

Furthermore, Ni_1Pd_1/CeO_2 can be reused for the decomposition of CFRP_MCDA several times. After the decomposition experiment of CFRP_MCDA, the catalyst can be easily separated from the carbon fiber by washing with acetone and water, benefiting from the different shape of the catalyst and the fiber (powder vs fiber). The recovered catalyst was washed with acetone, water and ethanol several times, followed by calcination at 300 °C under air for 3 h and H_2 for 1 h. Following these regeneration procedures, the catalyst was again subjected to the decomposition of CFRP_MCDA. As shown in Table 2, the catalyst can be reused at least 5 times without notable loss of its performance. After the 5th reuse experiment, 96% of the catalytic performance was still preserved compared to the decomposition experiment using the fresh catalyst. These experiments demonstrate the potential applicability of our catalyst system for the recovery of carbon fiber and phenolic compounds from CFRP_MCDA.

In summary, we have successfully developed the heterogeneous Ni–Pd/CeO_2 catalyst for the hydrogenolysis of epoxy resins. Notably, the catalyst can be applied to the decomposition of epoxy composites including CFRPs and the circuit board to recover phenolics and fibers.

https://doi.org/10.1038/s41467-025-56488-4

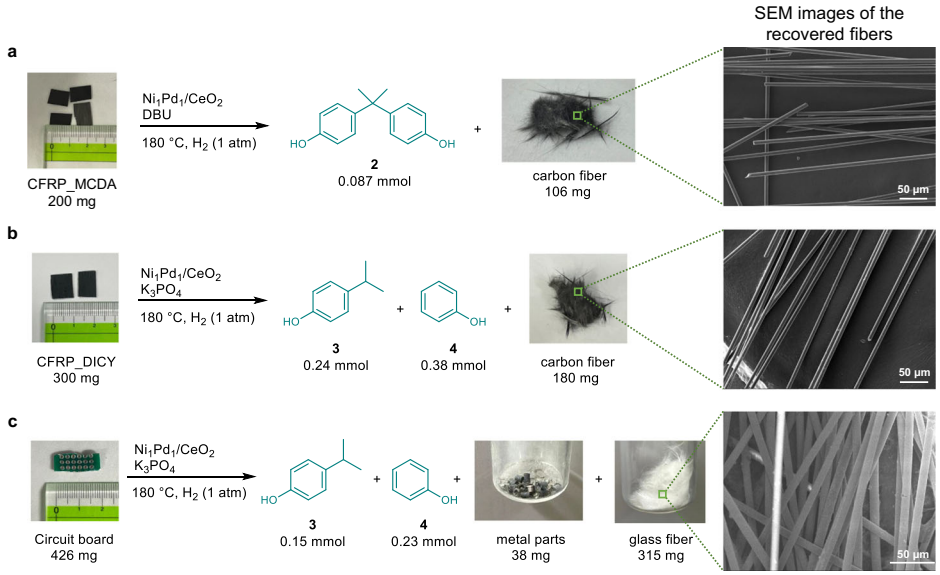

Fig. 6 | Ni_1Pd_1/CeO_2-promoted decomposition of epoxy composites. **a** Decomposition of CFRP_MCDA, and a SEM image of the carbon fiber recovered after the decomposition experiment. Reaction conditions: CFRP_MCDA (200 mg), Ni_1Pd_1/CeO_2 (100 mg), DBU (0.30 mmol), NMP (2.0 mL), 180 °C, H_2 (1 atm, balloon), 3 d. **b** Decomposition of CFRP_DICY, and a SEM image of the carbon fiber recovered after the decomposition experiment. Reaction conditions: CFRP_DICY (300 mg), Ni_1Pd_1/CeO_2 (100 mg), K_3PO_4 (0.50 mmol), NMP (2.0 mL), 180 °C, H_2 (1 atm, balloon), 3 d. **c** Decomposition of a circuit board (epoxy composite with glass fibers), and a SEM image of the glass fiber recovered after the decomposition experiment. Reaction conditions: circuit board piece (426 mg), Ni_1Pd_1/CeO_2 (100 mg), K_3PO_4 (0.50 mmol), NMP (2.0 mL), 180 °C, H_2 (1 atm, balloon), 3 d. For all the above experiments, Ni_1Pd_1/CeO_2 was pre-treated with 1 atm of H_2 at 300 °C for 1.0 h. Yields of the phenolic products were determined by GC analysis. Pictures of epoxy composites and recovered fibers or metal parts are shown.

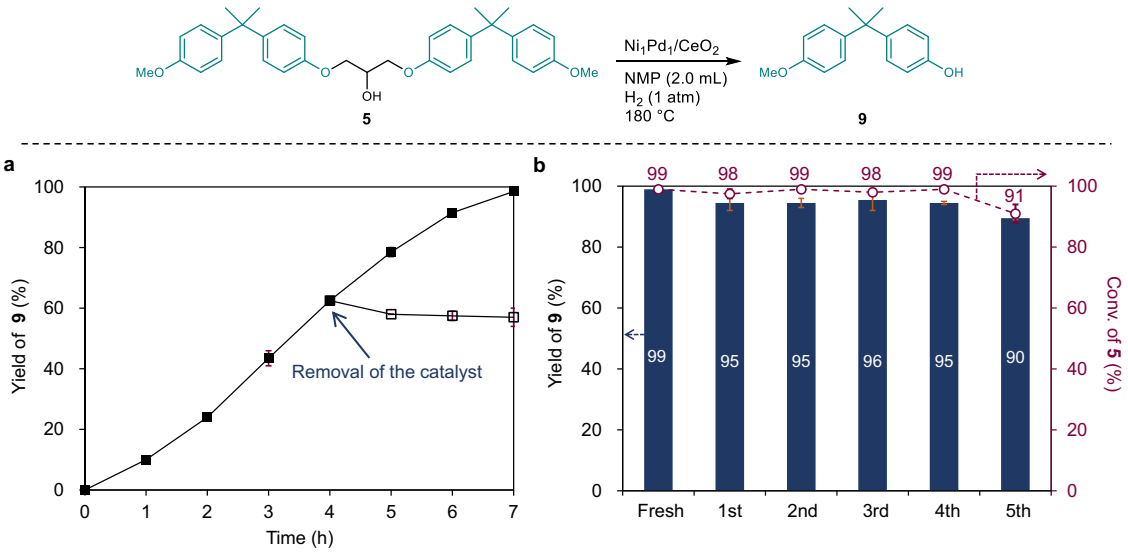

Fig. 7 | Leaching test and reuse of Ni_1Pd_1/CeO_2. **a** Effect of removal of the catalyst for the hydrogenolysis of model **5**. The filled squares indicate the yield of **9** without removal of the catalyst, and the open squares after removal of the catalyst by hot filtration. **b** Reuse experiments. After the reaction, the catalyst was retrieved by filtration, washed with acetone, water, and ethanol, dried at room temperature, and then applied to each reuse experiment. Reaction conditions: **5** (0.25 mmol), Ni_1Pd_1/CeO_2 (100 mg), NMP (2.0 mL), 180 °C, H_2 (1 atm, balloon), 7 h. For each experiment, the catalyst was pre-treated with 1 atm of H_2 at 300 °C for 1.0 h. The conversion and yields were determined by ^1H NMR and GC analysis, respectively. Each data point represents an average value of two parallel experiments, and standard deviations were added as error bars.

The catalyst can be recycled and reused several times even for the decomposition of the epoxy composite. Mechanistic studies suggested that the reaction proceeds through the dehydrogenation/hydrogenolysis sequences. In addition, while the Pd-induced reduction of Ni^{2+} to Ni^0 is the key to promoting dehydrogenation of the alcohol moiety, Pd species are mainly responsible for the C–O bond hydrogenolysis. The robustness and reusability of Ni–Pd/CeO_2 for the decomposition of CFRP imply its potential application in the recycling of epoxy composites.

Methods

Instruments and reagents

Gas chromatography (GC) analyses were performed on Shimadzu GC-2014 equipped with flame ionization detector (FID) and InertCap 5, 5MS/Sil capillary column. GC mass (GC–MS) spectra were recorded on Shimadzu GCMSQP2010 equipped with an InertCap 5MS/Sil capillary column at an ionization voltage of 70 eV. Nuclear magnetic resonance (NMR) spectra were recorded on BRUKER Ascend500 (^1H: 500 MHz, ^{13}C: 126 MHz) spectrometer at ambient temperature.

https://doi.org/10.1038/s41467-025-56488-4

Table 2 | Reuse of Ni_1Pd_1/CeO_2 for the decomposition of CFRP_MCDA

CFRP_MCDA

Entry	Catalyst	CFRP (mg)	Catalyst recovery (%)	Recovered carbon fiber (mg)	Yield of 2 (mmol)	Reusability compared to the fresh catalyst (%)
1	Fresh	200	92	106	0.087	-
2	1st reuse	192	92	106	0.080	95
3	2nd reuse	199	94	107	0.083	95
4	3rd reuse	201	96	106	0.084	97
5	4th reuse	205	92	102	0.083	93
6	5th reuse	204	93	103	0.085	96

Reaction conditions: CFRP_MCDA (approximately 200 mg), Ni_1Pd_1/CeO_2 (100 mg), DBU (0.30 mmol), NMP (2.0 mL), 180 °C, H_2 (1 atm, balloon), 3 d. The recovered catalyst was washed with acetone, water, and ethanol, and calcined at 300 °C under air for 3 h and H_2 for 1 h. The yield of **2** was determined by GC analysis. Pictures of CFRP_MCDA, and recovered fiber and catalyst are shown.

Chemical shift values for protons were determined using tetramethylsilane (TMS) (δ = 0 ppm) as the internal reference. Chemical shift values for carbons were determined using $CDCl_3$ (δ = 77.2 ppm) as the internal reference. High-resolution mass spectrum (HRMS) was taken with the electron spray ionization time-of-flight (ESI-TOF) method on JEOL JMS-T100LP AccuTOF LC-plus mass spectrometer. ICP-OES analyses were performed on a ThermoFisher iCAP PRO Duo. HADDF-STEM and EDS analysis were carried out using JEOL JEM-ARM 200F Thermal FE STEM operated at 200 kV. Powder X-ray diffraction (XRD) patterns were measured on a Rigaku Miniflex 600-C (CuKα, λ = 1.5406 Å, 40 kV, 15 mA). X-ray photoelectron spectroscopy (XPS) measurements were carried out on PHI5000 VersaProbe III using Al Kα radiation (hν = 1486.6 eV, 15 kV, 1.7 mA). The binding energies were calibrated by using the C 1*s* signal at 284.8 eV. Ni K-edge and Pd K-edge XANES measurements were performed at the BL01B1 beamline at SPring-8, which was operated at 8 GeV. A Si(111) and Si(311) double-crystal monochromator were used for Ni K-edge and Pd K-edge XANES measurements, respectively. The XAFS spectra were obtained at room temperature in transmittance or fluorescence mode. The data was reduced using xTunes (Science & Technology Institute Co.)[51]. Scanning electron microscopy (SEM) observation was performed on a JEOL JSM-7500FA. ZrO_2 (BET surface area: 279 $m^2\ g^{-1}$, JRC-ZRO-6), Al_2O_3 (BET surface area: 148 $m^2\ g^{-1}$, JRC-ALO-8), and TiO_2 (BET surface area: 269 $m^2\ g^{-1}$, JRC-TiO-14) are provided by Catalysis Society of Japan. CeO_2 (BET surface area: 111 $m^2\ g^{-1}$, Aldrich, cat no. 544841-25G) is commercially available. CFRP_MCDA and CFRP_DICY were kindly supplied by Toray Industries, Inc., for which epoxy resins cured with MCDA or DICY were used, respectively. The circuit board was commercially available (KAUMO universal board, double-sided through hole type, glass epoxy composite, 2.54 mm pitch, 2 × 8 cm; the composition of epoxy resin in the composite is unknown), which was cut into small pieces and used for the decomposition experiment. Solvents, substrates, and products were purchased from Kanto Chemical, TCI, Wako, or Aldrich, and used as received.

Preparation of Ni_1Pd_1/CeO_2

First, CeO_2 (2.0 g) was added to an aqueous solution (60 mL) of $NiCl_2$ (8.33 mM), $PdCl_2$ (8.33 mM), and KCl (2.0 equiv. with respect to $PdCl_2$, 16.7 mM). The resulting mixture was stirred vigorously at room temperature for 10 min, followed by adjusting the pH to 10 ± 0.5 using aqueous NaOH (1.0 M). After vigorous stirring at room temperature for 24 h, the solid was filtered off, washed with water (2.0 L), dried in vacuo, and pre-treated at 150°C and under H_2 (1 atm) for 0.5 h, affording the Ni_1Pd_1/CeO_2 catalyst (1.9 g, Pd contents: 0.25 mmol g^{-1}, 2.7 wt%, Ni contents: 0. 22 mmol g^{-1}, 1.3 wt%).

Typical procedures for the hydrogenolysis reaction (e.g., model 1)

Ni_1Pd_1/CeO_2 (100 mg) was added into a Schlenk tube (volume: ca. 20 mL) connected to a balloon filled with H_2 (1 atm). Then, the catalyst was pre-treated at 150 °C for 0.5 h. Following the pre-treatment, epoxy resin model **1** (200 mg, 0.52 mmol BPA unit), NMP (2.0 mL), and a Teflon-coated magnetic stir bar were successively added into the Schlenk tube under N_2 atmosphere. The reaction mixture was degassed twice by the freeze-pump-thaw method, and the Schenk tube was connected to a balloon filled with H_2. The reaction mixture was vigorously stirred at 180 °C for 12 h. After the reaction was completed, internal standards (1,1,2,2-tetrachloroethane and dodecane) were added to the reaction mixture. Conversion of **1** and yield of **4** were determined by ^1H NMR analysis using 1,1,2,2-tetrachloroethane as the internal standard, and yields of **2** and **3** were determined by GC analysis using dodecane as the internal standard.

Data availability

The data supporting the findings of this study are available within this article and its Supplementary Information file or from the authors upon reasonable request. Source data are provided with this paper.

References

1. Martín, A. J., Mondelli, C., Jaydev, S. D. & Pérez-Ramírez, J. Catalytic processing of plastic waste on the rise. *Chem* **7**, 1487–1533 (2021).
2. Ellis, L. D. et al. Chemical and biological catalysis for plastics recycling and upcycling. *Nat. Catal.* **4**, 539–556 (2021).
3. Korley, L. T. J., Epps, T. H., Helms, B. A. & Ryan, A. J. Toward polymer upcycling—adding value and tackling circularity. *Science* **373**, 66–69 (2021).
4. Lee, K., Jing, Y., Wang, Y. & Yan, N. A unified view on catalytic conversion of biomass and waste plastics. *Nat. Rev. Chem.* **6**, 635–652 (2022).
5. Pham, H. Q. & Marks, M. J. Epoxy resins in *Ullmann's Encyclopedia of Industrial Chemistry* (Wiley-VCH, 2005).
6. Shundo, A., Yamamoto, S. & Tanaka, K. Network formation and physical properties of epoxy resins for future practical applications. *JACS Au* **2**, 1522–1542 (2022).
7. Auvergne, R., Caillol, S., David, G., Boutevin, B. & Pascault, J.-P. Biobased thermosetting epoxy: present and future. *Chem. Rev.* **114**, 1082–1115 (2014).
8. Liu, Y. et al. Closed-loop chemical recycling of thermosetting polymers and their applications: a review. *Green Chem* **24**, 5691–5708 (2022).
9. Jiang, Y. et al. Bio-based hyperbranched epoxy resins: synthesis and recycling. *Chem. Soc. Rev.* **53**, 624–655 (2024).
10. Shen, Y., Apraku, S. E. & Zhu, Y. Recycling and recovery of fiber-reinforced polymer composites for end-of-life wind turbine blade management. *Green Chem* **25**, 9644–9658 (2023).
11. Li, Y. et al. Recycling of epoxy resins with degradable structures or dynamic cross-linking networks: a review. *Ind. Eng. Chem. Res.* **63**, 5005–5027 (2024).
12. Yang, W., Kim, K.-H. & Lee, J. Upcycling of decommissioned wind turbine blades through pyrolysis. *J. Clean. Prod.* **376**, 134292 (2022).
13. Li, J. et al. A promising strategy for chemical recycling of carbon fiber/thermoset composites: self-accelerating decomposition in a mild oxidative system. *Green Chem* **14**, 3260–3263 (2012).
14. Navarro, C. A. et al. Catalytic, aerobic depolymerization of epoxy thermoset composites. *Green Chem* **23**, 6356–6360 (2021).
15. Long, Y. et al. A mild and efficient oxidative degradation system of epoxy thermosets: full recovery and degradation mechanism. *Green Chem* **24**, 7082–7091 (2022).
16. Branfoot, C., Folkvord, H., Keith, M. & Leeke, G. A. Recovery of chemical recyclates from fibre-reinforced composites: a review of progress. *Polym. Degrad. Stab.* **215**, 110447 (2023).
17. DiPucchio, R. C., Stevenson, K. R., Lahive, C. W., Michener, W. E. & Beckham, G. T. Base-mediated depolymerization of amine-cured epoxy resins. *ACS Sustain. Chem. Eng.* **11**, 16946–16954 (2023).
18. Minami, Y. et al. Degradation of stable thermosetting epoxy resins mediated by bases in amide solvents. *Polym. J.* **57**, 149–162 (2025).
19. Sun, H. et al. Solvent–base mismatch enables the deconstruction of epoxy polymers and bisphenol A recovery. *Green Chem* **26**, 815–824 (2024).
20. Ahrens, A. et al. Catalytic disconnection of C–O bonds in epoxy resins and composites. *Nature* **617**, 730–737 (2023).
21. Ahrens, A. et al. Unveiling the mechanism of triphos-Ru catalysed C–O bond disconnections in polymers. *Nat. Commun.* **15**, 5656 (2024).
22. Liao, Y., Takahashi, K. & Nozaki, K. Nickel-catalyzed C(sp^3)–O hydrogenolysis via a remote-concerted oxidative addition and its application to degradation of a bisphenol A-based epoxy resin. *J. Am. Chem. Soc.* **146**, 2419–2425 (2024).
23. Eid, N., Ameduri, B. & Boutevin, B. Synthesis and properties of furan derivatives for epoxy resins. *ACS Sustain. Chem. Eng.* **9**, 8018–8031 (2021).
24. Türel, T., Dağlar, Ö., Eisenreich, F. & Tomović, Ž. Epoxy thermosets designed for chemical recycling. *Chem. Asian J.* **18**, e202300373 (2023).
25. Sergeev, A. G., Webb, J. D. & Hartwig, J. F. A heterogeneous nickel catalyst for the hydrogenolysis of aryl ethers without arene hydrogenation. *J. Am. Chem. Soc.* **134**, 20226–20229 (2012).
26. He, J., Zhao, C. & Lercher, J. A. Ni-catalyzed cleavage of aryl ethers in the aqueous phase. *J. Am. Chem. Soc.* **134**, 20768–20775 (2012).
27. Molinari, V., Giordano, C., Antonietti, M. & Esposito, D. Titanium nitride-nickel nanocomposite as heterogeneous catalyst for the hydrogenolysis of aryl ethers. *J. Am. Chem. Soc.* **136**, 1758–1761 (2014).
28. Sturgeon, M. R. et al. Lignin depolymerisation by nickel supported layered-double hydroxide catalysts. *Green Chem* **16**, 824–835 (2014).
29. Stavila, V. et al. MOF-based catalysts for selective hydrogenolysis of carbon–oxygen ether bonds. *ACS Catal.* **6**, 55–59 (2015).
30. Gao, F., Webb, J. D. & Hartwig, J. F. Chemo- and regioselective hydrogenolysis of diaryl ether C–O bonds by a robust heterogeneous Ni/C catalyst: applications to the cleavage of complex lignin-related fragments. *Angew. Chem. Int. Ed. Engl.* **55**, 1474–1478 (2016).
31. Schwob, T. et al. General and selective deoxygenation by hydrogen using a reusable earth-abundant metal catalyst. *Sci. Adv.* **5**, eaav3680 (2019).
32. Qi, L. et al. Unraveling the dynamic network in the reactions of an alkyl aryl ether catalyzed by Ni/γ-Al_2O_3 in 2-propanol. *J. Am. Chem. Soc.* **141**, 17370–17381 (2019).
33. Wang, M. et al. The critical role of reductive steps in the nickel-catalyzed hydrogenolysis and hydrolysis of aryl ether C–O bonds. *Angew. Chem. Int. Ed. Engl.* **59**, 1445–1449 (2020).
34. Jiang, L., Xu, G. & Fu, Y. Catalytic cleavage of the C–O bond in lignin and lignin-derived aryl ethers over Ni/AlP_yO_x catalysts. *ACS Catal.* **12**, 9473–9485 (2022).
35. Jin, X. et al. Metal–support cooperation in $Al(PO_3)_3$-supported platinum nanoparticles for the selective hydrogenolysis of phenols to arenes. *Nat. Catal.* **4**, 312–321 (2021).
36. Oshida, K. et al. Hydrogen-induced formation of surface acid sites on Pt/$Al(PO_3)_3$ enables remarkably efficient hydrogenolysis of C–O bonds in alcohols and ethers. *Angew. Chem. Int. Ed. Engl.* **63**, e202403092 (2024).
37. Alonso, D. M., Wettstein, S. G. & Dumesic, J. A. Bimetallic catalysts for upgrading of biomass to fuels and chemicals. *Chem. Soc. Rev.* **41**, 8075–8098 (2012).
38. Shivhare, A. et al. Hydrogenolysis of lignin-derived aromatic ethers over heterogeneous catalysts. *ACS Sustain. Chem. Eng.* **9**, 3379–3407 (2021).
39. Yun, Y. S., Berdugo-Díaz, C. E. & Flaherty, D. W. Advances in understanding the selective hydrogenolysis of biomass derivatives. *ACS Catal.* **11**, 11193–11232 (2021).
40. Liu, L. & Corma, A. Bimetallic sites for catalysis: from binuclear metal sites to bimetallic nanoclusters and nanoparticles. *Chem. Rev.* **123**, 4855–4933 (2023).
41. Zhang, J. et al. A series of NiM (M = Ru, Rh, and Pd) bimetallic catalysts for effective lignin hydrogenolysis in water. *ACS Catal.* **4**, 1574–1583 (2014).
42. Zhang, J. et al. Highly efficient, NiAu-catalyzed hydrogenolysis of lignin into phenolic chemicals. *Green Chem* **16**, 2432–2437 (2014).
43. Kim, J. K., Lee, J. K., Kang, K. H., Song, J. C. & Song, I. K. Selective cleavage of CO bond in benzyl phenyl ether to aromatics over Pd–Fe bimetallic catalyst supported on ordered mesoporous carbon. *Appl. Catal. A Gen.* **498**, 142–149 (2015).
44. Zhang, J.-w, Cai, Y., Lu, G.-p & Cai, C. Facile and selective hydrogenolysis of β-O-4 linkages in lignin catalyzed by Pd–Ni bimetallic nanoparticles supported on ZrO_2. *Green Chem* **18**, 6229–6235 (2016).

45. Zhang, J. et al. Rh nanoparticles with NiO_x surface decoration for selective hydrogenolysis of CO bond over arene hydrogenation. *J. Mol. Catal. A Chem.* **422**, 188–197 (2016).
46. Zhang, J.-w, Lu, G.-p & Cai, C. Self-hydrogen transfer hydrogenolysis of β-O-4 linkages in lignin catalyzed by MIL-100(Fe) supported Pd–Ni BMNPs. *Green Chem* **19**, 4538–4543 (2017).
47. Bulut, S. et al. Efficient cleavage of aryl ether C–O linkages by Rh–Ni and Ru–Ni nanoscale catalysts operating in water. *Chem. Sci.* **9**, 5530–5535 (2018).
48. Zhu, C. et al. Bimetallic effects in the catalytic hydrogenolysis of lignin and its model compounds on nickel-ruthenium catalysts. *Fuel Process. Technol.* **194**, 106126 (2019).
49. Kuang, X., Zhou, Y., Shi, Q., Wang, T. & Qi, H. J. Recycling of epoxy thermoset and composites via good solvent assisted and small molecules participated exchange reactions. *ACS Sustain. Chem. Eng.* **6**, 9189–9197 (2018).
50. Sheldon, R. A., Wallau, M., Arends, I. W. C. E. & Schuchardt, U. Heterogeneous catalysts for liquid-phase oxidations: philosophers' stones or Trojan horses? *Acc. Chem. Res.* **31**, 485–493 (1998).
51. Asakura, H. et al. xTunes: a new XAS processing tool for detailed and on-the-fly analysis. *Radiat. Phys. Chem.* **175**, 108270 (2020).

Acknowledgements

This work was supported by JST ERATO JPMJER2103 (K.Nozaki), and JSPS KAKENHI JP24K01253 (X.J.), JP23H04905 (X.J.). A part of this work was conducted at the Advanced Characterization Nanotechnology Platform of the University of Tokyo, supported by the "Nanotechnology Platform" of the Ministry of Education, Culture, Sports, Science and Technology (MEXT), Japan. The XAFS experiments at SPring-8 were carried out with the approval (proposal no. 2023B2023) of the Japan Synchrotron Radiation Research Institute (JASRI). We are grateful to S. Iwahana (Toray Industries, Inc.) and A. Masunaga (Toray Industries, Inc.) for kindly providing the CFRP sample. We would like to thank E. Amasawa (Waseda University) and E. Araki (U. Tokyo) for helping with the LCA analysis.

Author contributions

X.J. and K.Nozaki designed the studies and conceived the main idea. Y.H. and Y.Y. executed all the experimental works except for the XAFS measurements. K.Nomoto, H.M., and T.S. measured and analyzed the XAFS spectra. All authors discussed the results and wrote the paper.

Competing interests

The authors declare no competing interests.

Additional information

Supplementary information The online version contains supplementary material available at https://doi.org/10.1038/s41467-025-56488-4.

Correspondence and requests for materials should be addressed to Xiongjie Jin or Kyoko Nozaki.

Peer review information *Nature Communications* thanks Alexander Ahrens and Yao Fu for their contribution to the peer review of this work. A peer review file is available.